Sparse Autoencoder Based Manifold Analyzer Model of Multi-Angle Target Feature

XIUYUAN CHEN[ID][1,2], **XIYUAN PENG**[ID][1,2], **JUN-BAO LI**[1,2], **AND CHAOYING HUO**[3]

[1]Harbin Institute of Technology, Harbin 150080, China
[2]School of Electronics and Information Engineering, Harbin Institute of Technology, Harbin 150080, China
[3]Science and Technology on Electromagnetic Scattering Laboratory, Beijing 100039, China

Corresponding author: Jun-Bao Li (junbaolihit@126.com)

ABSTRACT Automatic target recognition (ATR) has always been an important research topic, and the performance is affected by feature extraction. High-resolution range profiles (HRRP) contains structural information of target from different angles. Existing target recognition algorithms are mostly adopt the supervised learning and verify the validity through classification accuracy. However, these methods cannot satisfy the information acquisition such as correlation, composition analysis and attitude analysis of unlabeled or uncoordinated targets. Therefore, we are committed to researching new intelligent feature extraction and analysis method. In this article, a novel learning framework is proposed to realize the angle correlation feature extraction and feature analysis of multi-angle HRRP targets. A multi-layer sparse autoencoder is applied to extract HRRP features and the extracted features are mapped to the low-dimensional space by manifold learning method to find the correlation distribution of HRRP data. The effectiveness of the proposed framework is demonstrated by experiments with simulated and measured data. The experimental results show that the framework realizes the extraction of angle-invariant features, and the analysis of distribution relationship between HRRP data and angles. The research results of the correspondence between the assembly and the related geometry provide the basis and possibility for further identification and composition determination.

INDEX TERMS ATR, feature extraction, HRRP, manifold analyzer, sparse autoencoder.

I. INTRODUCTION

High-resolution range profiles (HRRP) is the magnitude of coherent summations of the complex time return from target scatters along the radar line of sight. Since HRRP data are relatively easy to acquire and process and provide plenty of information, many researches have been developed based on HRRP in recent years [1]. In [2], deep network structure is introduced to solve the problem of target recognition, while researchers [3], [4] adopt traditional methods such as dictionary learning and decision tree. In [5], multi-kernel learning is introduced to improve the nonlinear ability of the classifier, and a new adaptive method [6] is proposed based on the small sample characteristics of HRRP data.

The associate editor coordinating the review of this manuscript and approving it for publication was Jingchang Huang[ID].

In the previous studies, researchers mostly adopted the supervised training methods commonly used in pattern recognition and the most likely label prediction was given according to some evaluation rules. However, HRRP target recognition research has its own challenge. The target recognition of radar HRRP is quite different from that of our daily objects or visible images. Firstly, radar target recognition is a single-sample recognition task, and each type of target is the data obtained by a single object from different angles. Therefore, the difference within the class is only the azimuth difference in data acquisition. Secondly, the research object samples in HRRP recognition are not completely independent from each other, and each sample is generally acquired along a certain trajectory, so there is a certain spatiotemporal correlativity of these samples. In the actual recognition task, it is rare to obtain the complete

label of the recognition object, so the recognition needs to start from feature analysis. The geometric characteristics of targets and the distribution of strong scattering points in HRRP data are generally affected by such properties as amplitude sensitivity, translation sensitivity and azimuth sensitivity. Azimuth sensitivity usually establishes the data and corresponding template by dividing the specific angle area, which may not completely reflect the target properties. In addition, when the target is a non-matching or non-fixed category of objects and the labels in the training library are unable to give accurate recognition results, it is more helpful to identify the target by analyzing the target components and giving the information of possible components of the target than simply giving a certain classification label. In view of the characteristics and existing problems of the above HRRP target recognition task, we consider the solution of this problem from a new perspective. Instead of classifying the objects in the way of supervised learning and training, we are committed to extracting the angle-related features and analyzing the possible component in HRRP target.

Therefore, regardless of the applications of HRRP, the extraction and interpretation of features are critical, and the quality of extracted features affects the performance of HRRP-related applications. Many scholars have spent much effort studying the methods of HRRP feature extraction. Some researchers [7], [8] have used complicated statistical models to extract HRRP features, which have specific physical meaning, such as the target size, center of gravity, and number of peaks. Using super-resolution algorithms, the precise location and intensity information of radar HRRP scatterers can be extracted [9], [10]. However, the effects of these feature-based extraction methods are highly dependent on the experience of the researchers, which will cause the extracted features to be incomplete or to deviate without sufficient prior knowledge. In contrast, the data-driven feature extraction method eliminates human interference and directly obtains accurate information from the data. In [11], a subspace model is established to realize feature extraction based on principal components analysis (PCA). Manifold learning is used in target recognition of radar HRRP to reduce the feature dimensions [12]. These methods map high-dimensional data to low-dimensional space and realize feature extraction by data dimensionality reduction.

At present, many common methods of dimensionality reduction are divided into linear and nonlinear algorithms. The algorithm performance of linear dimensionality reduction methods, such as PCA, linear discriminate analysis (LDA) [13], and multidimensional scaling (MDS) [14], are limited by the linear characteristics of the method, especially for radar signals, which contain much noise information; the effect may not be ideal. Isomap [15], Laplacian eigenmaps (LE) [16], and locally linear embedding (LLE) [17] are typical nonlinear algorithms. Some new dimensionality reduction methods have been proposed to solve the classification of hyperspectral images [18], [19]. However, we are more concerned about nonlinear dimensionality reduction

methods belong to the category of manifold learning, whose goal is to find low-dimensional manifolds embedded in high-dimensional space. Manifold mapping needs to satisfy the homeomorphic mapping relationship between two spaces, which is consistent with our goal of studying the low-dimensional spatial distribution of radar signals. However, when looking for angle invariance, a large number of high-dimensional spatial data need to be mapped to a few low-dimensional spatial points, which is inconsistent with the injective conditions in homeomorphic mapping. An important component of machine learning, the autoencoder plays an important role in unsupervised learning and nonlinear feature extraction. As a good feature extraction structure, autoencoder is used in combination with many other methods, such as extreme learning machine (ELM) [20] and some traditional classifiers, for target recognition. The improved autoencoder with different regularization constraints, such as sparse autoencoder has better performance in various target recognition studies [21]. Therefore, we adopt the autoencoder method to achieve dimensionality reduction and find the low-dimensional angle invariance features of high-dimensional HRRP data. In [22], manifold learning method is combined with antoencoder, but the goal of this article is to improve the performance of autoencoder. Our goal of combining the two methods is to form a novel framework for the extraction and analysis of target angle-related features and component correlation.

The framework is proposed to analyze the angle correlation characteristics of HRRP data from the perspective of feature extraction and analysis, and looks for the corresponding relationship between assembly and corresponding geometry. In this way, the angle-invariance feature and the angular mapping relationship of HRRP data in the low-dimensional space are obtained. This method can be used to realize the analysis of non-specific angle targets, extract the angle relevant characteristics of target, and extract the features of non-cooperative or non-specific types of targets with some common features, and put forward identification suggestions. This article is composed as follows. Chapter two introduces the HRRP feature extraction and analysis framework proposed in this article, as well as the algorithm and principle of related functions. Chapter three introduces the experimental data set making, experimental design and analysis. Chapter four is the summary and prospect of future work.

II. ALGORITHM

A. FRAMEWORK

In this article, we propose a novel feature extraction and analysis framework to realize the multi-angle HRRP target feature extraction and analysis function. Through a multi-layer sparse autoencoder, feature extraction of HRRP data is realized by unsupervised learning. Then, the manifold mapping is introduced to map the HRRP features into a low-dimensional space to obtain the distribution of HRRP data in the low-dimensional space for characteristic analysis.
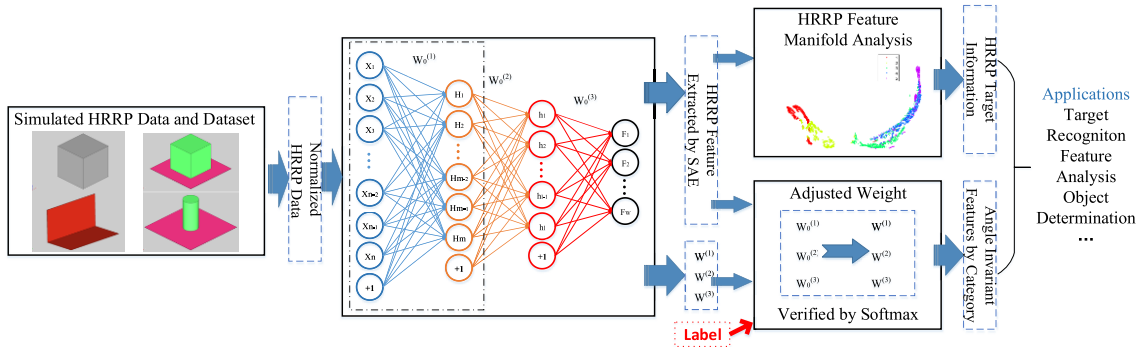
FIGURE 1. Overall flow chart of our proposed framework.

Supervised training is conducted on the previously obtained features to extract the angle invariance of HRRP targets. After encoding the HRRP data of a class of targets from different angles into angle-invariant feature vectors, the vector performance is tested by the classifier. The overall flow chart of the proposed framework is shown in Fig. 1.

Therefore, this framework mainly realizes the following three contents:

1. Data dimensionality reduction and feature extraction: 1024-dimensional HRRP radar target data obtained by simulation are reduced to 30-dimensional output features via a multi-layer sparse autoencoder.
2. HRRP feature manifold mapping: the 30-dimensional features obtained by unsupervised learning are taken as input to study the manifold distribution of high-dimensional features in low-dimensional (2-dimensional and 3-dimensional) spaces.
3. Angle-invariant feature extraction: After the new network parameters are acquired by supervised learning, the angle-invariant features can be converted from 1024-dimensional data to 30-dimensional features, and then the softmax classifier verifies the validity of the features.

The research object of the experiment in this article is to obtain basic geometry data by simulation. The data-related details and data set construction rules will be introduced in the following chapters. This chapter mainly explains the related algorithms of feature dimension reduction, network parameter optimization and manifold mapping within the framework.

B. STEP 1: HRRP DIMENSIONALITY REDUCTION

The HRRP of a certain target under a certain pitch and horizontal angle obtained by simulation is a 1024-dimensional vector, and each dimension represents the intensity in the width upward. After the HRRP data are formed into a dataset according to certain rules, a multi-layer sparse autoencoder is used for data dimensionality reduction and feature extraction. An autoencoder is an artificial neural network that can obtain efficient representation of input data through unsupervised learning. The unsupervision of the autoencoder lies in that

after encoding and decoding input data, network parameter training can be completed by minimizing reconstruction errors.

$$y = f_{\theta 1}(x) = s(W_1 x + b_1) \tag{1}$$

$$z = f_{\theta 2}(y) = s(W_2 y + b_2) \tag{2}$$

$$\min L = J(W, b) = \frac{1}{m} \sum_{i=1}^{m} \frac{1}{2} \|x_i - z_i\|^2 \tag{3}$$

where s is a nonlinear function, and the sigmoid function is used as the activation function in this article. (1) and (2) are the encoding and decoding processes, respectively. Input x is transformed into the activation value of the hidden layer and then reversely transformed into a reconstruction representation z of the original input. $\theta 1 = \{W_1, b_1\}$ and $\theta 2 = \{W_2, b_2\}$ are the sets of parameters for two transformations. (3) is the loss function of the autoencoder, and the minimization is to make the representation z infinitely close to x. The loss function can be minimized by repeated iteration, and the main information and characteristics of the samples can be retained in the coding process.

There are many applications and improvements of autoencoder, but in the demand for learning features, especially for recognition features, sparse autoencoder is often adopted. In this article, sparse expression is introduced to obtain unique statistical features that reflect the training dataset, rather than just finding identity functions in the coding and decoding process. Through this learning process, replication tasks with sparse punishment can be performed to obtain models that can learn useful features. In addition to obtaining the parameter sets, the sparse autoencoder also needs to solve the average activity of neurons in the hidden layer in the coding and decoding process:

$$\hat{\rho}_j = \frac{1}{m} \sum_{i=1}^{m} \left[\alpha_j \left(x^{(i)} \right) \right] \tag{4}$$

The $\alpha_j(x)$ is used to indicate the activation of the hidden neuron j given an input of x and m is the number of hidden neurons. When the average activity of a hidden neuron is small, it can be considered to optimize it by introducing the
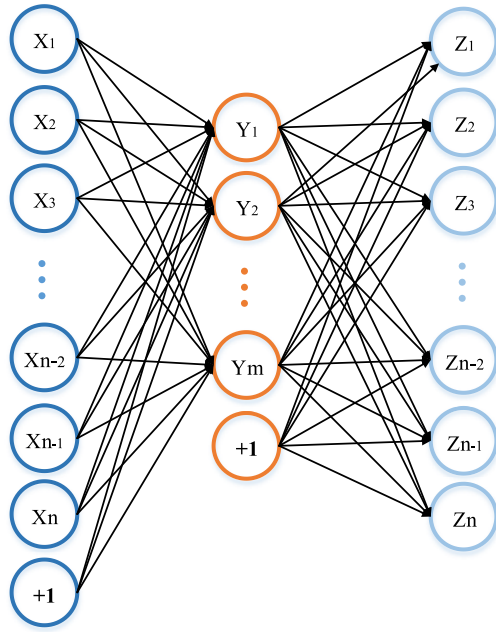
FIGURE 2. The sparse autoencoder.

sparsity restriction ρ. In this article, we set the value of this variable to 0.1 for each layer. The additional sparse penalty factor is added to the loss function to be optimized through the sparse constraint condition and the Kullback-Leibler Divergence (KL) is introduced to measure the similarity between the average activity output ρ_j of a hidden node j and the sparse restriction:

$$\mathrm{KL}\left(\rho \,\|\, \hat{\rho}_j\right) = \rho \log \frac{\rho}{\hat{\rho}_j} + (1 - \rho) \log \frac{1 - \rho}{1 - \hat{\rho}_j} \qquad (5)$$

$$J_{\mathrm{sparse}}\left(W, b\right) = J\left(W, b\right) + \beta \sum_{j=1}^{m} \mathrm{KL}\left(\rho \,\|\, \hat{\rho}_j\right) \qquad (6)$$

(6) is the function of the optimal value of the final demand solution. Parameters W and b are updated to obtain the optimal solution through iteration. In traditional learning algorithms, the gradient descent method is often used to solve the optimal value, but in the optimal solution of high-dimensional data, the convergence speed is slow. Therefore, the L-BFGS (L means limited memory) algorithm is adopted in this article to solve network parameters. The L-BFGS algorithm is an optimization of the traditional BFGS algorithm, which approximates the inverse of the Hessian matrix with a matrix without the second derivative. The iteration formula of the estimated inverse Hessian matrix $B = H^{-1}$ is as follows:

$$B_{k+1} = V_k^{\mathrm{T}} B_k V_k + \rho_k s_k s_k^{\mathrm{T}} \qquad (7)$$

where $V_k = 1 - \rho_k y_k s_k^{\mathrm{T}}$, $\rho_k = 1/\left(y_k^{\mathrm{T}} s_k\right)$, $y_k = g_{k+1} - g_k$, $g_k = \nabla f\left(x_k\right)$, $B_k = r_k I$, $r_k = \left(s_{k-1}^{\mathrm{T}} y_{k-1}\right) / \left(y_{k-1}^{\mathrm{T}} y_{k-1}\right)$, $s_k = x_{k+1} - x_k$. $\nabla f\left(x_k\right)$ is the gradient of the objective function at x_k. Then, for the kth iteration, if only the information of the

last m iterations is retained, the expression becomes:

$$
\begin{aligned}
B_k = {} & \left(V_{k-1}^{\mathrm{T}} \cdots V_{k-m}^{\mathrm{T}}\right) B_k \left(V_{k-m} \cdots V_{k-1}\right) \\
& + \left(V_{k-1}^{\mathrm{T}} \cdots V_{k-m+1}^{\mathrm{T}}\right) s_{k-m} \rho_{k-m} s_{k-m}^{\mathrm{T}} \\
& \times \left(V_{k-m+1} \cdots V_{k-1}\right) \\
& + \left(V_{k-1}^{\mathrm{T}} \cdots V_{k-m+2}^{\mathrm{T}}\right) s_{k-m+1} \rho_{k-m+1} s_{k-m+1}^{\mathrm{T}} \\
& \times \left(V_{k-m+2} \cdots V_{k-1}\right) \\
& + \cdots + s_{k-1} \rho_{k-1} s_{k-1}^{\mathrm{T}} \qquad (8)
\end{aligned}
$$

Then, L-BFGS only needs to record m vectors to construct an approximate matrix, thus reducing the memory footprint and computational complexity and improving the convergence speed. The pseud-code of L-BFGS optimization algorithm is as follows:

Step 1: Initial point x_0, initialize $k = 0$, $H_0 = I$, $r = \nabla f\left(x_0\right)$
Step 2: Compute the iteration direction $p_k = -r_k$
Step 3: Compute the step length α_k, then search for $f\left(x_k + \alpha_k p_k\right) = \min_{\alpha \geq 0}\left(x_k + \alpha_k p_k\right)$
Step 4: Update the weights
Step 5: If $k > m$, then start to save the most recent mth vector pairs
Step 6: Compute and save
Step 7: Compute $r_k = H_k \nabla f\left(x_k\right)$, $k = k+1$
Step 8: If $\|\nabla f\left(x_{k+1}\right)\| \leq \varepsilon$ then return the optimal solution, else go to Step 2.

By taking the hidden layer of the sparse autoencoder as the input layer of the next autoencoder, multiple autoencoders can be stacked to form a deep structure, which can compress or extract the data features layer by layer for analysis and subsequent application. In this article, a three-layer sparse autoencoder is adopted, and the number of hidden layers is set to 256 and 128. The output features of the multi-layer self-encoder (dimension is set to 30) are the unsupervised learning features obtained.

C. STEP 2: HRRP FEATURE MANIFOLD MAPPING

After obtaining the 30-dimensional features from the multi-layer sparse encoder, this article completes the extraction and visualization of the target angle features by using low-dimensional spatial mapping through manifold learning. From the introduction of the first part, the common dimensionality reduction algorithms are divided into linear and nonlinear. The complexity of the radar working environment and echo and the noise in the HRRP data make the data and characteristics highly nonlinear. Therefore, the t-distributed stochastic neighbor embedding (t-SNE) algorithm [23] with the best performance among the nonlinear methods is adopted in this article. t-SNE measures the distribution characteristics of the data in two spaces by calculating the distribution probability density between samples in high-low dimensional space. The t-SNE algorithm used in this step is to convert Euclidean distance into conditional probability to express

the similarity between points. The probability distribution of high-dimensional data is constructed, and the amount of data adjacent to each data point is set by perplexity. Then the probability distribution of these data points is constructed in the low-dimensional space, and the two probability distributions are made as similar as possible through iterative training. While achieving homeomorphism mapping, the manifold distribution of high-dimensional data in low-dimensional space is obtained. For high-dimensional data, that is, the 30-dimensional HRRP features obtained through unsupervised learning in this article, the conditional probability distribution of any two vectors is first calculated:

$$p_{j|i} = \frac{\exp\left(-\left\|x_i - x_j\right\|^2 \Big/ 2\sigma_i^2\right)}{\sum_{k \neq i} \exp\left(-\left\|x_i - x_k\right\|^2 \Big/ 2\sigma_i^2\right)} \quad (9)$$

$p_{j|i}$ represents the similarity between the data points x_i and x_j. The parameter σ_i is the Gussian mean square deviation centered on x_i. The joint probability density of HRRP features in high-dimensional space is calculated according to the conditional probability distribution, and the joint probability density q_{ij} and gradient $\partial C / \partial Y$ of low-dimensional space are calculated by using the t distribution with 1 degree of freedom.

$$p_{ij} = \frac{p_{j|i} + p_{i|j}}{2n} \quad (10)$$

$$q_{ij} = \frac{\left(1 + \left\|y_i - y_j\right\|^2\right)^{-1}}{\sum_{k \neq l} \left(1 + \left\|y_k - y_l\right\|^2\right)^{-1}} \quad (11)$$

$$C = KL\left(P \| Q\right) = \sum_i \sum_j p_{ij} \log \frac{p_{ij}}{q_{ij}} \quad (12)$$

$$\frac{\delta C}{\delta y_i} = 4 \sum_j \left(p_{ij} - q_{ij}\right)\left(y_i - y_j\right) \quad (13)$$

where C is the loss function defined by the Kullback-Leibler Divergence (KL) distance, and each iteration needs to calculate whether the loss function reaches the minimum value to determine the optimal solution. During the experimental process in this article, when dimension reduction of HRRP features is carried out in some cases, the loss function will continue to decline, but the final decline rate is extremely slow. When the number of iterations is set to the maximum value, the increase in time complexity does not significantly increase the efficiency, so the number of iterations in this article is set to 400. The pseud-code of t-SNE algorithm is as follows:

Step 1: Input Data: X = {x₁,x₂,...,xₙ}, initialize the number of iterations T, learning rate η, momentum α(t)
Step 2: Compute the parameter Perp of cost function
Step 3: Compute the conditional probability $p_{j|i}$ under Perp with formula (9)
Step 4: Compute formula (10)
Step 5: Randomly initialize Y with $N(0, 10^{-4}I)$

Step 6: Iteration from t = 1 to T
      Compute formula (11)-(13)
      Update Yᵗ
Step 7: End

D. STEP 3: ANGLE-INVARIANT FEATURE EXTRACTION

HRRP data have a strong angle sensitivity, but in some classification and recognition tasks, there is a need to eliminate or reduce the differences caused by the angle within the class and ensure that the differences between classes are not affected to maintain large differences between classes. In the third step, we achieved this goal through supervised learning and extracted the angle-invariant features of HRRP data.

We used the unsupervised learning parameters $W_0 = \left\{W_0^{(1)}, W_0^{(2)}, W_0^{(3)}\right\}$ and $b_0 = \left\{b_0^{(1)}, b_0^{(2)}, b_0^{(3)}\right\}$ as the initialization parameters and obtained the adjusted parameters $W = \left\{W^{(1)}, W^{(2)}, W^{(3)}\right\}$ and $b = \left\{b^{(1)}, b^{(2)}, b^{(3)}\right\}$ by supervised learning. The HRRP data extraction process in the proposed framework can obtain a 30-dimensional feature that can be used to identify and distinguish between classes. The training data set constructed in this article is the radar HRRP data under an elevation angle of 0 to 90 degrees and a horizontal angle of 0 to 90 degrees. Therefore, for a certain class of targets, the unified features obtained under supervision training are the angle-invariant features of these targets. A softmax classifier was used to verify the effectiveness of the feature extraction in this step.

III. EXPERIMENT AND RESULT ANALYSIS
A. SIMULATED DATA AND DATASET

The experimental HRRP data used in this article is composed of simulation data and measured data. The simulation data of geometry and combinations are derived from electromagnetic simulation. The parameters are an X-band center frequency of 10 GHz, a bandwidth of 2 GB, a frequency interval of 10 MHz, and the polarization mode adopted HH polarization. The range of the pitch angle is 0∼90°, and the angle interval is 10°. The horizontal angle is 0∼90°, and the angle interval is 0.05°. Thus, there are 18010 multi-angle HRRP data for each type of target. This article studies five types of typical geometry, namely, cube, cylinder, dihedral angle, trihedral angle and cone, and four other combinations. The geometric shapes and related parameters are as follows:

Figure 4 and Figure 5 have high similarity in geometry. However, in HRRP, when several components are combined, the imaging will change to some extent due to the increase in the reflection times, which means a simple object as an individual is different from a component in HRRP data. As shown in Fig. 6 and Fig. 7, we present the HRRP images of the cube and trihedral in three angles and compare them to the combination at the corresponding angle.

In HRRP data, the peak value and number of strong scattering points will change at different azimuth angles. As we show in Fig. 6 and Fig. 7, the cube's number of
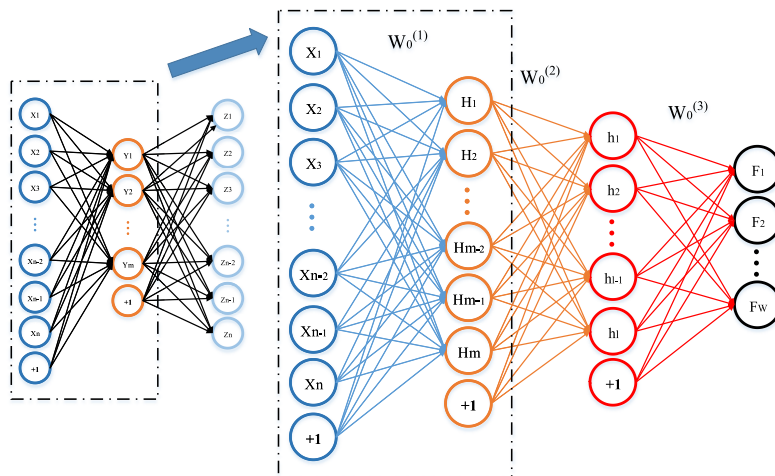
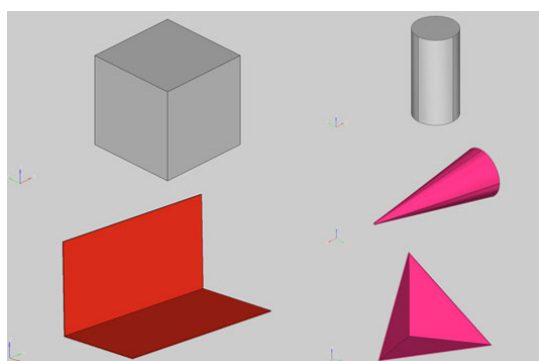**FIGURE 3.** The multi-layer sparse autoencoder.
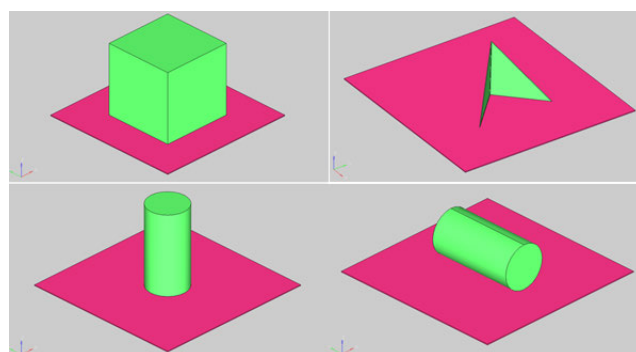

FIGURE 4. The geometric shapes of typical geometry.

FIGURE 5. The geometric shapes of combinations.

TABLE 1. Geometric parameters and information.

Geometry	Geometric Sizes	Coordinate Center	Modeling Method
Cube	Side length: 1 m	Geometric Center	PO+EEC
Trihedral angle	Side length: 600 mm, Thickness: 5 mm	Vertex of Angle	PO+EEC+SBR
Dihedral angle	Size: 1 m×0.5 m, Thickness: 5 mm	Angular Center	PO+EEC+SBR
Cylinder	Diameter: 0.5 m, Height: 1 m	Bottom Center	PO+EEC
Cone	Height: 3257.804 mm, Bottom Diameter: 1200 mm, Cone Angle: 10°	Bottom Center	PO+EEC

TABLE 2. Information for combination.

Combination	Modeling Method	Blanking Method
Plate-Cube	PO+EEC+SBR	Ray-Casting, Z-Buffer
Plate-Trihedral	PO+EEC+SBR	Ray-Casting, Z-Buffer
Plate-Cylinder (stand)	PO+EEC+SBR	Ray-Casting, Z-Buffer
Plate-Cylinder (lying)	PO+EEC+SBR	Ray-Casting, Z-Buffer

strong scattering points and peak value vary at different angles in HRRP data. In addition, there is a strong similarity between the cube and the trihedral in HRRP data at some certain angles. Therefore, we focus on two points in the analysis of Angle characteristics: one is the angle-invariant feature used for recognition, and the other is the angle-based low-dimensional spatial distribution in the class. For the analysis of the basic composition of complex objects, we also consider the simple geometry and the geometry on the plate as two types to analyze their relevance in the feature space.

To construct the training set and test set, 6000 data are extracted from 18010 data of each type, of which 4000 are training data and 2000 are verification data, so the training set size is 20000, and the verification set size is 10000. The sampling rules for constructing the data set are as follows: 600 data were selected evenly from 1801 data by evenly selecting ten reference angles, and 60 data were selected at intervals of 0.05 degrees around each reference angle. Forty of the 60 data points were randomly selected into the training set, and the others were selected into the test set. To further
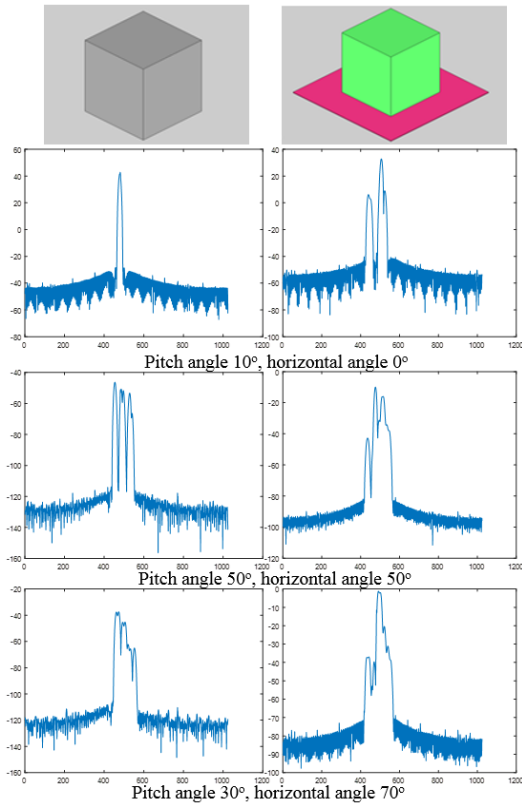
FIGURE 6. The HRRP of cube and cube with plate.

FIGURE 7. The HRRP of trihedral and trihedral with plate.

TABLE 3. Information for MSTAR dataset.

	Training Set	Test Set
t72	4000	2000
btr70	4000	2000
brdm2	4000	2000
bmp2	4000	2000

verify the effectiveness of the target angle-invariant feature extracted by the method in this article, 200 data from each category were randomly selected as supplementary validation data sets in the remaining data.

In order to verify the performance of the method in complex measured data, four kinds of ground vehicle data in MSTAR data (t72, btr70, brdm2, and bmp2) are selected as research objects. MSTAR data is the currently available and most widely used ground stationary target data of SAR. Many researches on SAR image target recognition are carried out based on this data. In recognition studies, 128*128 slice images obtained after signal processing are mostly used, while the data we used were processed into HRRP data for experiment. The visual images and corresponding HRRP data are shown in Fig. 8. The data was collected at elevation angles of 17° and horizontal angles of 0° to 360°, and the sampling interval is 0.2°. Target names and the number of samples in training and test set are shown in table 3.

B. EXPERIMENTAL DESIGN AND OBJECTIVES

To verify the performance of the HRRP feature extraction and analysis framework proposed in this article, the extracted features need to be displayed, and the validity of the features should be verified through classification. In this article, after the training of a multi-layer sparse autoencoder model, the validation set is used to classify five categories of simple geometry to verify t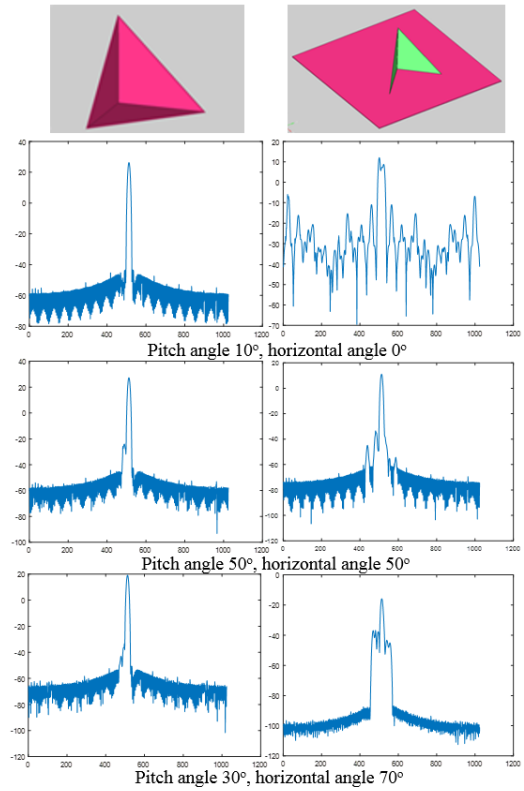he validity of angle-invariant features that can be used to distinguish between classes. In addition, for the features extracted from the unsupervised part, the results are analyzed in a visual way, and the specific contents are as follows:

a. Verify the validity of the features by classifying the test sets and sorting the angle-invariant feature vectors, which can also be called category labels;

b. Visualize the feature vectors of each layer obtained from unsupervised and supervised training to compare and elaborate the extracted feature of each layer from a multi-layer sparse autoencoder;

c. Visually display the dimensionality reduction features of the unsupervised learning part in three-dimensional space and observe the distribution and characteristics of their changes with angle and category;

d. Visually display the dimensionality reduction features of the unsupervised learning part in two-dimensional space and observe the changes in its distribution and characteristics with angle;
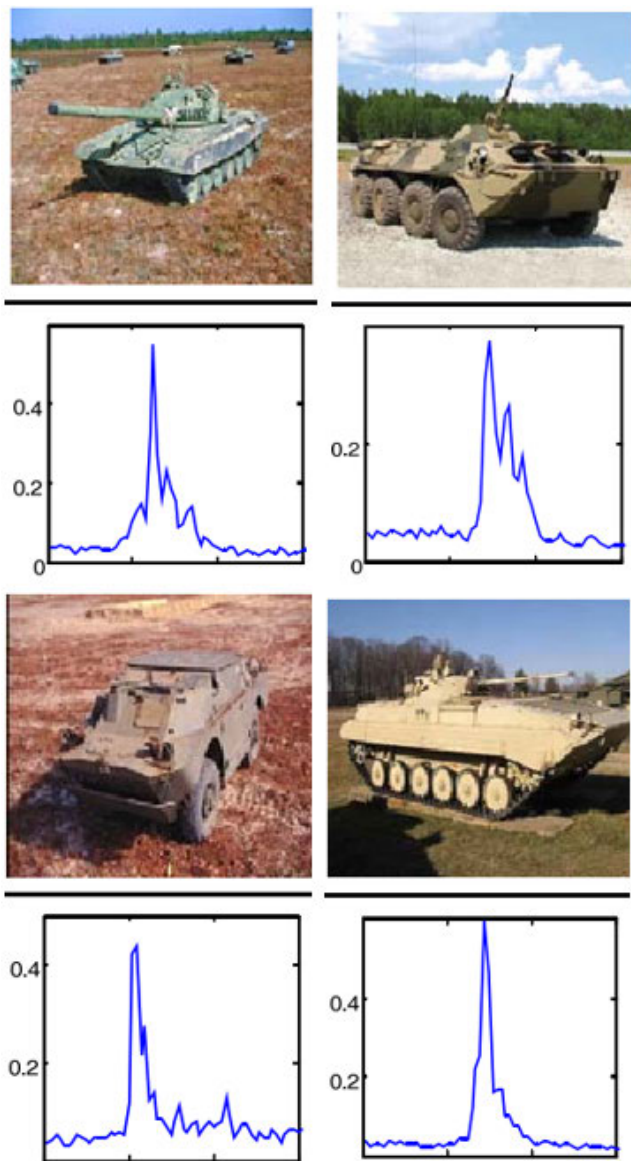
FIGURE 8. The visual images and HRRP of four kinds of MSTAR.

e. Visually display the dimensionality reduction features of the combination in two-dimensional and three-dimensional spaces, observe the differences with the typical geometry, and analyze the distribution changes and feature analysis of the geometric component.

C. RESULTS AND DISCUSSION

Our experiments are conducted in Matlab, and we use computer with CPU cores for computing. The multi-layer sparse autoencoder adopted in this article is a three-layer network. The input data are 1024-dimensional HRRP data, and the dimensions of the hidden layer characteristics are 256 and 128. In this way, each data is output as a 30-dimensional eigenvector through the network. After the model parameters are adjusted through the labeled supervision training, the output through the network is also an

adjusted feature. The features are sent into softmax to classify the five types of basic geometry. The classification accuracy is 99.80% on the test set and 98.86% on the supplementary validation set. In MSTAR data, we achieve the classification accuracy of 99.6%, which means our structure can also achieve good feature extraction ability for complex objects. Since the data set is constructed from HRRP data in full angle and the angle of supplementary validation set is different from that of the training set and test set, the classification results prove that the strong classification features obtained by the method proposed in this article have angle invariance. That is, the 30-dimensional eigenvector obtained from the target data through the supervised learning part of the framework is only relevant to the target category and does not change with the changes in pitch and azimuth angle. The angle-invariant features of typical geometry and MSTAR targets are shown in Table 4 and Table 5:

TABLE 4. The angle-invariant features of typical geometry.

Geometry	The Angle-invariant Feature
Cube	110011,010001,100100,000000,110010
Cylinder	011000,001001,000111,010110,001100
Dihedral angle	000000,001101,100001,111001,001000
Cone	000011,101100,100110,000011,001001
Trihedral angle	000101,000010,111001,100101,000100

TABLE 5. The angle-invariant features of MSTAR targets.

TARGET	The Angle-invariant Feature
T72	110000,000000,101100,001100,000010
BTR70	000100,011001,000111,010110,001100
BRDM2	010010,000101,000001,100011,001010
BMP2	101001,110000,100110,010000,011001

Therefore, the high accuracy in classification comes from the angle-invariant feature in binary form. To explore the source of good performance of the features, the features obtained from unsupervised and supervised learning are visualized and analyzed layer by layer. The comparison results are shown in Fig. 9.
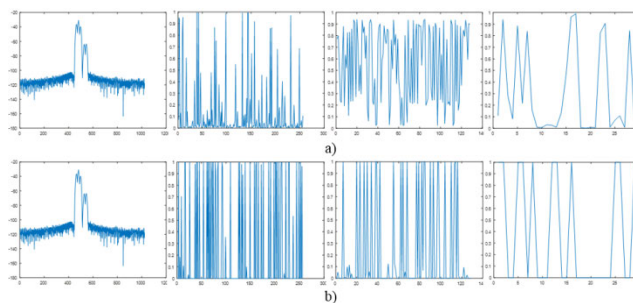

FIGURE 9. a) Unsupervised and b) supervised feature.

The comparison of visual features shows that the features obtained by supervised learning are the further normalization of unsupervised features and that the features are enhanced by label-based training to eliminate the angle differences within the class. From the perspective of feature mapping in space, the supervised learning part of the framework further converges the points originally mapped to the 30-dimensional feature space to five points in the space. Therefore, features obtained by sparse autoencoders also have certain properties, while we observe the properties by visualizing the features of HRRP data in three-dimensional space. 3-D visualization results of five types of geometry targets and MSTAR targets are shown in Fig. 10 and Fig. 11.

a) SAE+LLE
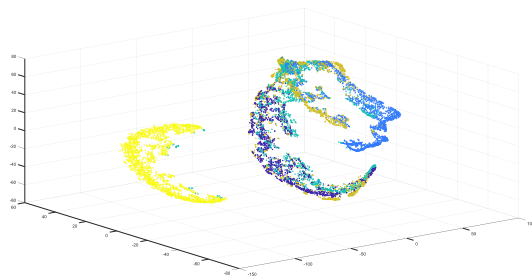
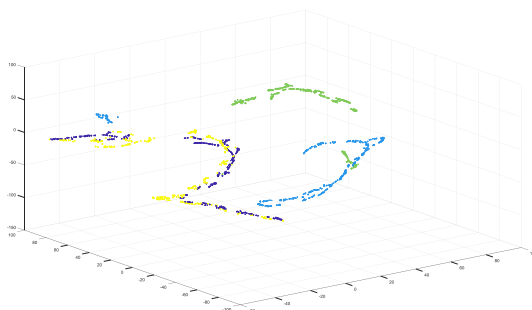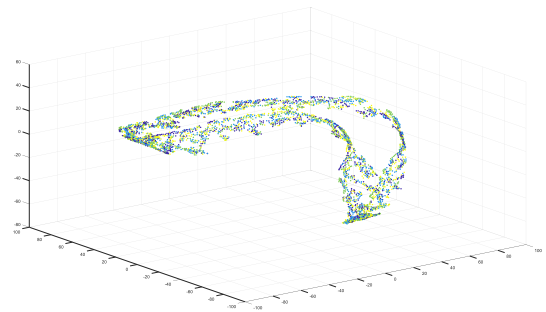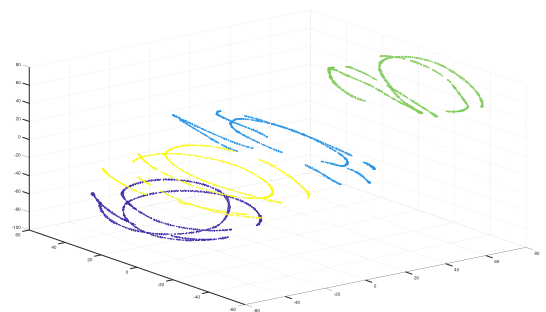**FIGURE 10.** 3-D visualization result of five types of geometry targets.

b) t-SNE

FIGURE 11. 3-D visualization result of four MSTAR targets.

c) SAE+t-SNE

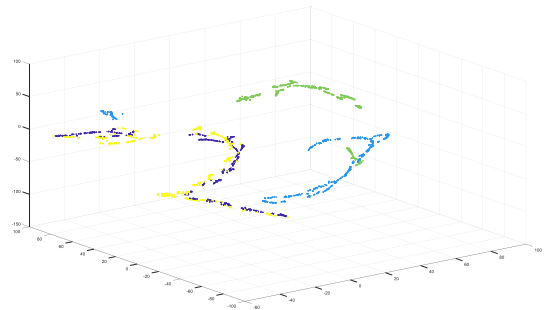**FIGURE 12.** 3-D visualization result comparison of different manifold methods.

The purpose of our research is to explore the distribution characteristics of high-dimensional HRRP data in low-dimensional space, analyze and mine the attitude sensitivity of the target. Therefore, we compare the mapping results of our proposed SAE+ t-sne with those of SAE+LLE and t-sne in low-dimensional space, as shown in Fig. 12. Comparing figure a) and c), it can be seen that under the framework proposed in this article, t-sne algorithm has better separability than LLE algorithm. As can be seen from figure a), certain distribution characteristics can be extracted through SAE. However, due to poor performance of LLE or the inapplicability of LLE to HRRP data, the mapping from the high-dimensional space to the low-dimensional space results in the overlap between the distributions. In contrast, one advantage of the t-sne algorithm is that it can enlarge the distance between low-correlated or irrelevant samples after mapping to a low-dimensional space. Therefore, the

separability of t-sne in figure b) is good, but there is no spatial distribution of the angle feature extracted by SAE. The classification effect in figure c) is not as good as that in figure b), but it combines the advantages of a) and b), and it can be seen from the previous verification of angle invariance that although the spatial distance is relatively close, it is still separable.

Each point in the figure represents an HRRP sample, and the five colors represent five types of typical geometry. The figure shows that the features obtained by unsupervised learning are also separable to some extent and have a manifold distribution in 3-d space. The acquisition and simulation of HRRP data are all based on the azimuth

angle. We further analyze the characteristics and explore the relationship between low-dimensional manifold and azimuth in high-dimensional space. For each category of data, the 3-d mapping of its distribution by pitch angle is visualized first, and the results are shown in the figure below.

Each figure in Fig. 13 shows the results of visualization of dimensionality reduction features obtained by unsupervised learning of five types of simple bodies in three-dimensional space. The data points with a pitch angle of 0°, 30°, 60° and 90° and a horizontal angle of 0° to 90° are listed here for illustration. The data at different pitching angles are located in different low-dimensional spaces, so the data in the class have certain separability at the pitching angles. The search for two-dimensional low-dimensional manifold distribution at horizontal angles continues in the same pitching angles and the results are shown in Fig. 14-17.

The number means that the data points in the figure are divided into five groups of horizontal angles from 0° to 90°. The data points are represented by different colors to denote the relationship between distribution and horizontal angles. As we introduced in the last paragraph, the data points with a pitch angle of 0°, 30°, 60° and 90° are listed for illustration. The four subgraphs correspond in turn to the low-dimensional mapping results under four pitch angles from 0° to 90° in Fig. 14-17. The four subgraphs of each figure are to prove that, at different pitch angles, the high-dimensional data of various geometric objects mapped to two-dimensional space have manifold distributions related to horizontal angles. In most subgraphs, the low-dimensional mapping results obtained through the architecture have a good distribution by horizontal Angle, but some poor distribution do occur (the first subgraphs in Figure 14-16). Although the mapping effect is different, the mapping conforms to the gradual feature under the change in horizontal angle. The horizontal angle of the target data can be confirmed and analyzed through feature mapping, and the dimensionality reduction features extracted by this framework can provide corresponding information in aspects of angle analysis, trajectory analysis and category analysis.

Therefore, the visual analysis of the characteristics of unsupervised learning shows that the architecture proposed in this article has obvious angle discrimination and low-dimensional manifold distribution for multi-angle HRRP targets. The results of the data under different pitching angles in three-dimensional space prove that the data from the same category are in different low-dimensional manifolds according to the division of the pitching angles, while the data of the same pitching angle have a certain order distribution in two-dimensional space according to the horizontal angle. The two-dimensional distribution between different categories also has obvious differences. Therefore, the object can also be estimated and identified in terms of angles and categories to some extent without labels.

In this article, a research object is positioned as a typical geometry because the latter can represent the local obvious
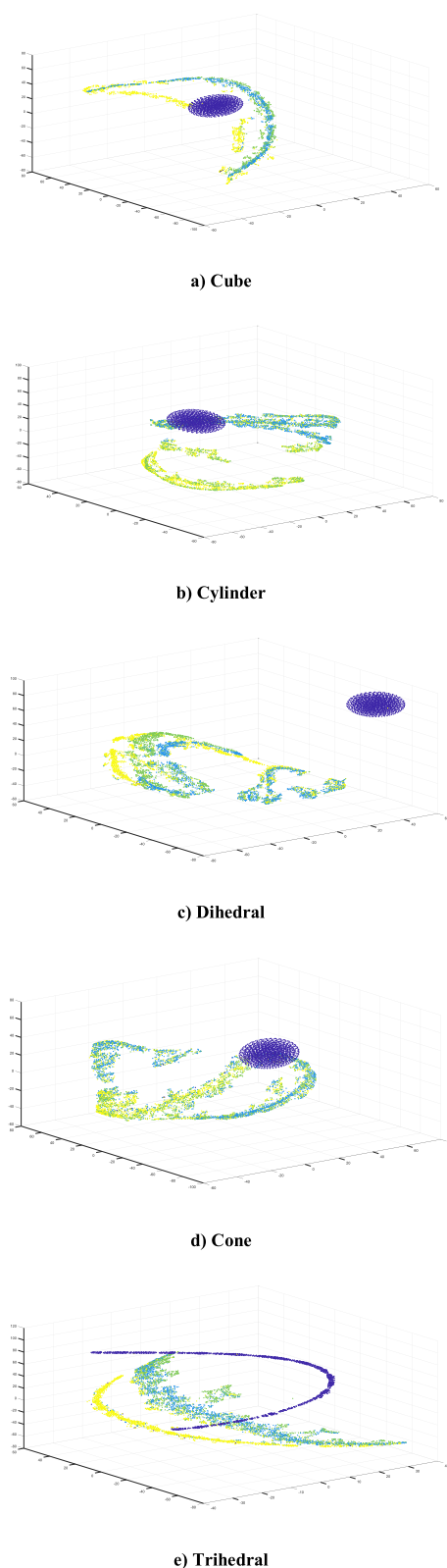

a) Cube

b) Cylinder

c) Dihedral

d) Cone

e) Trihedral

FIGURE 13. 3-D visualization result of single class displayed by pitch angle.

characteristics of complex objects. In radar target recognition and characteristic analysis, modeling and training complete
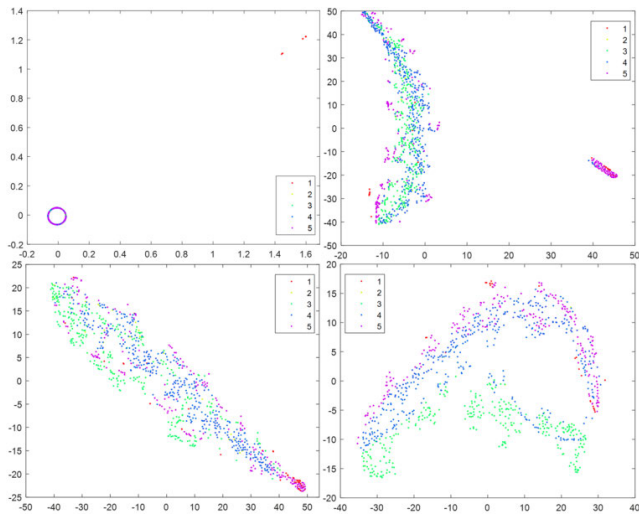
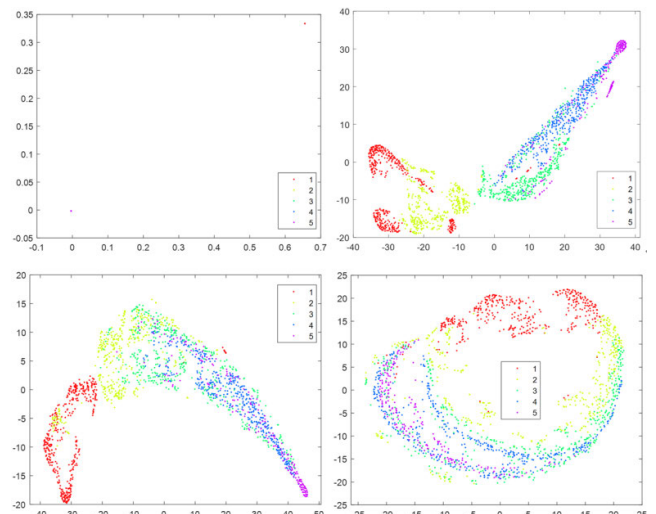**FIGURE 14.** 2-D visualization results of cube under four pitching angles.

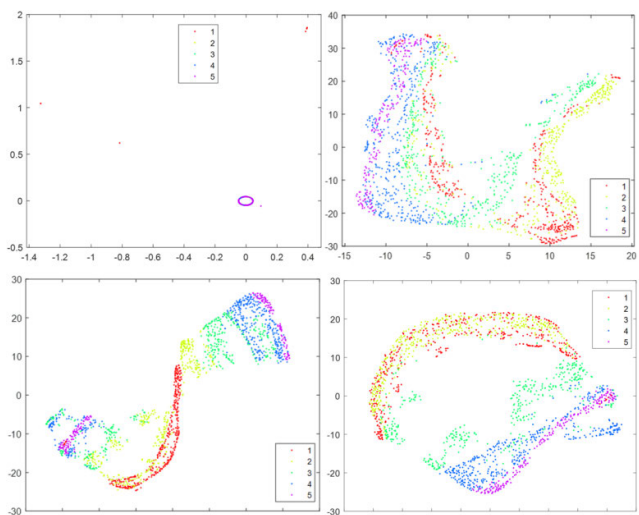**FIGURE 16.** 2-D visualization results of dihedral under four pitching angles.

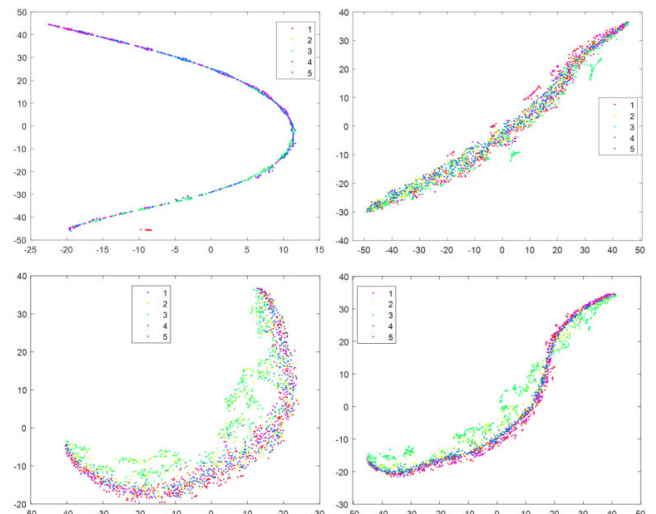**FIGURE 15.** 2-D visualization results of cylinder under four pitching angles.

FIGURE 17. 2-D visualization results of trihedral under four pitching angles.

target categories in some practical situations is impossible, or the identification requirements of some parts are higher than that of the whole in the identification process. Therefore, in addition to studying a typical geometry, this article also simulates the construction of plate-typical geometry assembly data to simulate the detection effect of components in the overall local position. The HRRP data of the assembly are introduced into the trained model, and the dimensionality reduction visualization of the output features is carried out to analyze the distribution relationship between the features and the typical geometry.

Each subgraph in Fig. 18-20 is the low-dimensional mapping result of typical geometry and corresponding assembly under the same angle condition. There are two placement modes of the cylinder in the assembly, so the corresponding subgraphs contain three mapping results of

a geometry and two assembly. Fig. 18 is a full-angle three-dimensional diagram of three simple bodies (cube, trihedral, and cylinder) and the assembly. In Fig. 6 and Fig. 7, we show the difference between geometry and their corresponding assembly in HRRP image and the confusion of different objects in specific angle. In Fig. 18 a) and b), there is a strong similarity between geometry and the corresponding assembly in the mapping of low-dimensional space, which shows the corresponding relationship between geometry and assembly in feature analysis. Although the distortion of the cylinder in the mapping of the assembly is obvious, the distribution results are still helpful for the feature analysis of recognition. The results shown in Fig. 19 and Fig. 20 are the comparisons in the two-dimensional mapping space, which proves the high-dimensional data of assembly mapped to
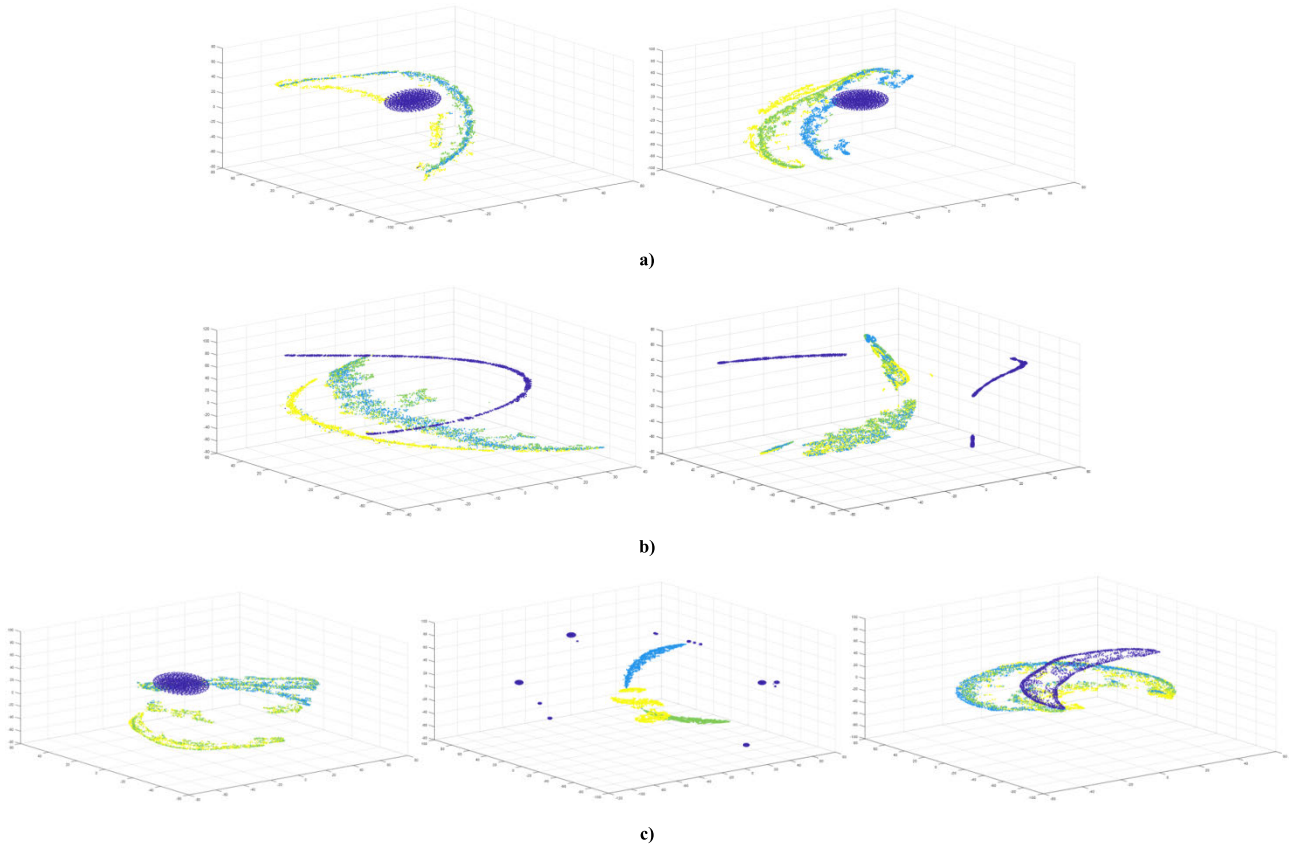
FIGURE 18. 3-D visualization comparison between the assembly and the origin. a) Cube, b) trihedral and c) cylinder.

a) Pitch angle of 0° b) Pitch angle of 30°

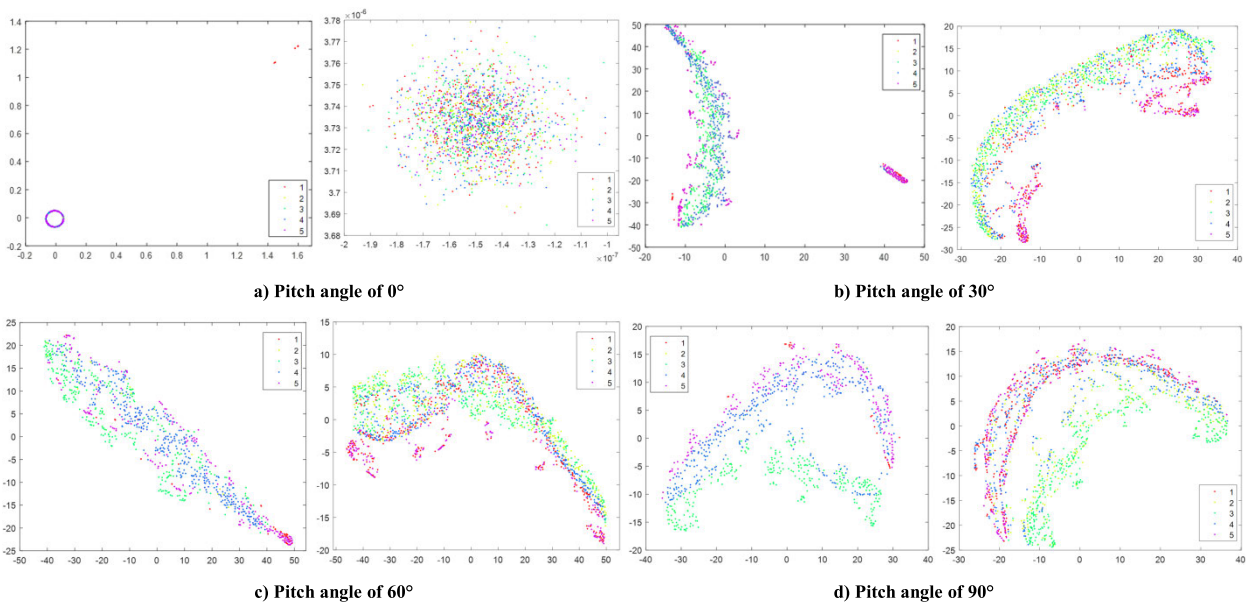c) Pitch angle of 60° d) Pitch angle of 90°

FIGURE 19. 2-D visualization comparison between the plate-cube and the original cube.

two-dimensional space have manifold distributions related to horizontal angles and the mapping of geometry and assembly has a certain similarity at the same pitch angle. In this part,

the results show that the framework proposed in this article plays a certain role in identifying the basic component in the assembly.
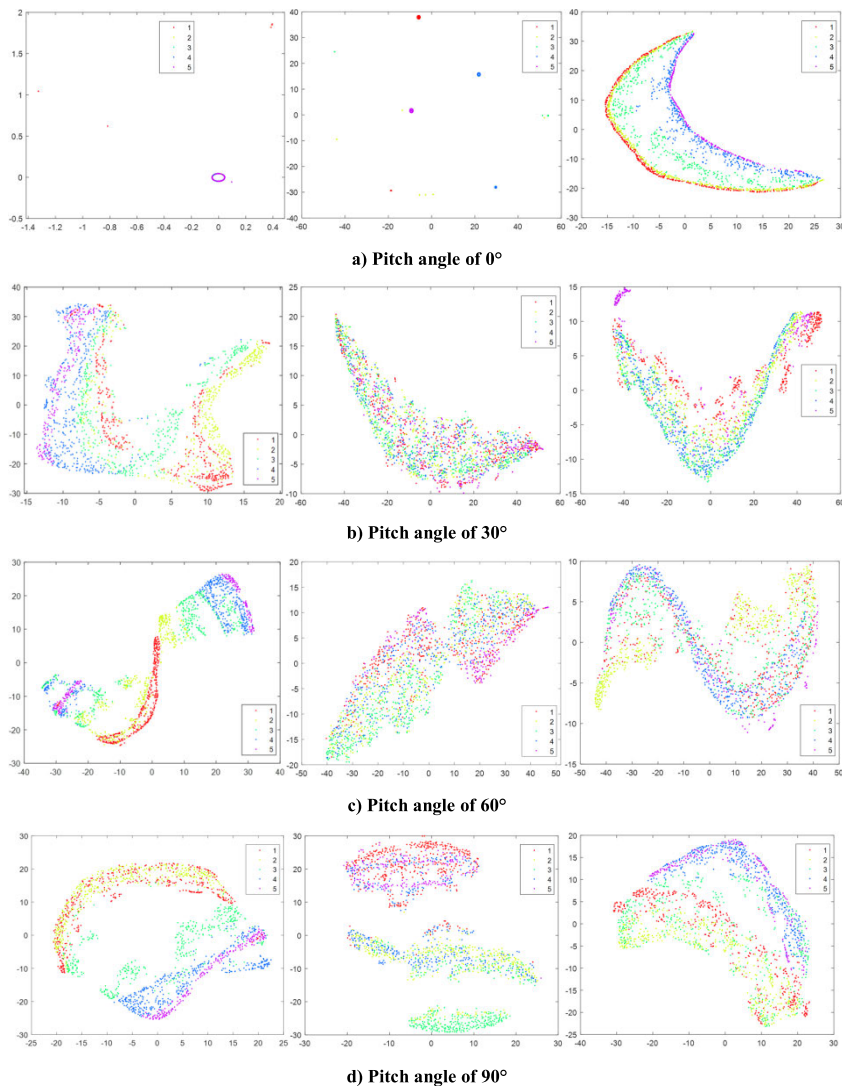
a) Pitch angle of 0°

b) Pitch angle of 30°

c) Pitch angle of 60°

d) Pitch angle of 90°

FIGURE 20. 2-D visualization comparison between the plate-cylinder and the original cylinder.

IV. CONCLUSION

In this article, we realize the analysis of angle related features and low-dimensional distribution of multi-angle HRRP targets, and study the relationship between the assembly and corresponding geometry in low-dimensional distribution. The contribution of this article lies in the construction of a novel framework, which extracts features from HRRP data and uses manifold learning method to mapping into low-dimensional space, and analyzes the features. Firstly, the angle-invariant feature obtained after fine-tuning proves the uniqueness of each target, which indicates that the research on HRRP target recognition can be carried out from non-specific angles. Secondly, the results of low-dimensional distribution after feature extraction and mapping show that the HRRP data corresponding to the data points in the low-dimensional space conform to a certain distribution with the pitch angle and horizontal angle. Finally, it can be seen from the comparison experiment of the combination and corresponding geometry

that although there is a big difference in HRRP data, there is a strong correlation between them in the low-dimensional distribution obtained by mapping. The above findings provide the possibility for multi-angle target analysis and component feature analysis. In the future, we will further optimize our framework for more complex environments, and improve the algorithm to achieve better results.

REFERENCES

[1] X.-Y. Pan, W. Wang, and G.-Y. Wang, "Sub-Nyquist sampling jamming against ISAR with CS-based HRRP reconstruction," *IEEE Sensors J.*, vol. 16, no. 6, pp. 1597–1602, Mar. 2016.

[2] B. Feng, B. Chen, and H. Liu, "Radar HRRP target recognition with deep networks," *Pattern Recognit.*, vol. 61, pp. 379–393, Jan. 2017.

[3] D. Zhou, "Radar target HRRP recognition based on reconstructive and discriminative dictionary learning," *Signal Process.*, vol. 126, pp. 52–64, Sep. 2016.

[4] S. Wang, J. Li, Y. Wang, and Y. Li, "Radar HRRP target recognition based on gradient boosting decision tree," in *Proc. 9th Int. Congr. Image Signal Process., Biomed. Eng. Informat. (CISP-BMEI)*, Oct. 2016, pp. 1013–1017.

[5] W. Xiong, G. Zhang, S. Liu, and J. Yin, "Multiscale kernel sparse coding-based classifier for HRRP radar target recognition," *IET Radar, Sonar Navigat.*, vol. 10, no. 9, pp. 1594–1602, Dec. 2016.

[6] B. Feng, L. Du, C. Shao, P. Wang, and H. Liu, "Radar HRRP target recognition based on robust dictionary learning with small training data size," in *Proc. IEEE Radar Conf. (RADAR)*, Apr. 2013, pp. 1–4.

[7] S. Slomka, D. Gibbins, D. Gray, and B. Haywood, "Features for high resolution radar range profile based ship classification," in *Proc. 5th Int. Symp. Signal Process. Appl. (ISSPA)*, 1999, pp. 329–332.

[8] C. M. Pilcher and A. Khotanzad, "Maritime ATR using classifier combination and high resolution range profiles," *IEEE Trans. Aerosp. Electron. Syst.*, vol. 47, no. 4, pp. 2558–2573, Oct. 2011.

[9] J. Li and P. Stoica, "Efficient mixed-spectrum estimation with applications to target feature extraction," *IEEE Trans. Signal Process*, vol. 42, no. 2, pp. 281–295, Feb. 1996.

[10] B. Pei and Z. Bao, "Multi-aspect radar target recognition method based on scattering centers and HMMs classifiers," *IEEE Trans. Aerosp. Electron. Syst.*, vol. 41, no. 3, pp. 1067–1074, Jul. 2005.

[11] L. Du, H. Liu, Z. Bao, and J. Zhang, "Radar automatic target recognition using complex high-resolution range profiles," *IET Radar, Sonar Navigat.*, vol. 1, no. 1, pp. 18–26, Feb. 2007.

[12] L. Li and Z. Liu, "Noise-robust HRRP target recognition method via sparse-low-rank representation," *Electron. Lett.*, vol. 53, no. 24, pp. 1602–1604, Nov. 2017.

[13] W. Wang and M. Zhang, "Face recognition based on symmetrical linear discriminate analysis," *J. Comput. Appl.*, vol. 29, no. 12, pp. 3352–3353, Mar. 2010.

[14] R. N. Shepard, "Multidimensional scaling, tree-fitting, and clustering," *Science*, vol. 210, no. 4468, pp. 390–398, Oct. 1980.

[15] J. B. Tenenbaum, "A global geometric framework for nonlinear dimensionality reduction," *Science*, vol. 290, no. 5500, pp. 2319–2323, Dec. 2000.

[16] M. Belkin and P. Niyogi, "Convergence of Laplacian eigenmaps," in *Proc. Conf. Adv. Neural Inf. Process. Syst.*, 2006, pp. 129–136.

[17] S. T. Roweis, "Nonlinear dimensionality reduction by locally linear embedding," *Science*, vol. 290, no. 5500, pp. 2323–2326, Dec. 2000.

[18] F. Luo, L. Zhang, X. Zhou, T. Guo, Y. Cheng, and T. Yin, "Sparse-adaptive hypergraph discriminant analysis for hyperspectral image classification," *IEEE Geosci. Remote Sens. Lett.*, vol. 17, no. 6, pp. 1082–1086, Jun. 2020.

[19] F. Luo, L. Zhang, B. Du, and L. Zhang, "Dimensionality reduction with enhanced hybrid-graph discriminant learning for hyperspectral image classification," *IEEE Trans. Geosci. Remote Sens.*, vol. 58, no. 8, pp. 5336–5353, Aug. 2020.

[20] G.-B. Huang, Q.-Y. Zhu, and C.-K. Siew, "Extreme learning machine: Theory and applications," *Neurocomputing*, vol. 70, nos. 1–3, pp. 489–501, Dec. 2006.

[21] F. Guo, J. Huang, X. Zhang, X. You, X. Zu, Q. Zhao, Y. Ding, H. Liu, and B. Li, "A classification method for moving targets in the wild based on microphone array and linear sparse auto-encoder," *Neurocomputing*, vol. 241, pp. 28–37, Jun. 2017.

[22] Q. Yang and F. Sun, "Small sample learning with high order contractive auto-encoders and application in SAR images," *Sci. China Inf. Sci.*, vol. 61, no. 9, pp. 218–306, Sep. 2018.

[23] L. van der Maaten and G. Hinton, "Visualizing data using t-SNE," *J. Mach. Learn. Res.*, vol. 9, no. 2605, pp. 2579–2605, Nov. 2008.

XIUYUAN CHEN received the B.S. degree in measuring and control instrument from the Harbin Institute of Technology, Harbin, China, in 2012, where he is currently pursuing the Ph.D. degree with the Automatic Test and Control Institute. His research interests include pattern recognition, target recognition based on semi-supervised learning, and radar target analysis.

XIYUAN PENG received the B.S., M.S., and Ph.D. degrees from HIT, Harbin, China, in 1984, 1987, and 1992, respectively. He is currently a Full Professor with the School of Electronics and Information Engineering, HIT. His current research interests include automatic test and advanced fault diagnostics technology.

JUN-BAO LI received the Ph.D. degree in pattern recognition from the Harbin Institute of Technology, China, in 2008. He is currently a Full Professor with the School of Electronics and Information Engineering, Harbin Institute of Technology. His research interests include deep learning, kernel learning and applications (kernel optimization; kernel sparse learning; kernel manifold learning; supervised kernel self-adaptive learning; and applications of kernel learning), and medical image processing and classification (segmentation, enhance, and feature extraction of medical image; and mammogram-based breast cancer diagnosis). He has authored more than 80 articles, including 60 SCI journals in pattern recognition areas.

CHAOYING HUO received the M.S. degree from the Graduate School of Second Academy of Aerospace Science and Engineering. She is currently a Research Fellow with the Science and Technology on Electromagnetic Scattering Laboratory. Her research interests include radar feature extraction and application technology.

● ● ●